Nucleic Acids Research, 2006, Vol. 34, No. 8 ***e64***
doi:10.1093/nar/gkl291

Hydroxyl radical footprinting *in vivo*: mapping macromolecular structures with synchrotron radiation

Tadepalli Adilakshmi, Richard A. Lease and Sarah A. Woodson*

T.C. Jenkins Department of Biophysics, Johns Hopkins University, 3400 North Charles Street, Baltimore, MD 21218, USA

Received March 8, 2006; Revised and Accepted April 6, 2006

ABSTRACT

We used a high flux synchrotron X-ray beam to map the structure of 16S rRNA and RNase P in viable bacteria *in situ*. A 300 ms exposure to the X-ray beam was sufficient for optimal cleavage of the phosphodiester backbone. The *in vivo* footprints of the 16S rRNA in frozen cells were similar to those obtained *in vitro* and were consistent with the predicted accessibility of the RNA backbone to hydroxyl radical. Protection or enhanced cleavage of certain nucleotides *in vivo* can be explained by interactions with tRNA and perturbation of the subunit interface. Thus, short exposures to a synchrotron X-ray beam can footprint the tertiary structure and protein contacts of RNA–protein complexes with nucleotide resolution in living cells.

INTRODUCTION

The functions of many DNA or RNA complexes are linked to biochemical and structural changes during assembly and intracellular transport. Assembly and transport are in turn regulated by cell signaling or environmental cues. Methods for determining the structure of macromolecules *in situ* under a variety of growth conditions can capture such structural changes within the cell. Chemical reagents such as dimethylsulphate (DMS) and lead (II) acetate, and kethoxal (1–7), KMnO4 (8), and copper-phenanthroline (9) have been used to probe the structures of nucleic acids *in vivo*. These reagents are primarily sensitive to secondary structure or local backbone flexibility. In contrast, hydroxyl radical footprinting is useful for 3D modeling because it provides information on tertiary structure and intermolecular interfaces with single nucleotide resolution (10).

We used X-rays from a high flux synchrotron beam to generate hydroxyl radical and probe the structure of rRNA and RNase P inside viable *Escherichia coli* cells. This method has been used for time-resolved footprinting of RNA structure *in vitro* (11). The radiolysis of water by X-rays produces free electrons and hydroxyl radicals (12), which can abstract a hydrogen atom from the ribose sugar and initiate cleavage of the polynucleotide backbone (13,14). Deuterium isotope studies (15) and comparisons with known RNA structures (16–18) showed that the hydroxyl radical cleavage pattern correlates with the solvent accessibility of the backbone hydrogen atoms.

The production of hydroxyl radical and other diffusible radicals is a principal cause of radiation damage to biological samples (13,14). Water contributes 70% of the cell's mass, and virtually all the X-rays absorbed by the cell are captured by water, limiting direct damage to cellular components. Because X-rays easily penetrate cells and soft tissue, they can be used to generate hydroxyl radical in intact cells without permeabilizing the membranes. A 15 min exposure to a ^{137}Cs gamma ray source was used previously to footprint lambda repressor–DNA complexes *in vivo* (19). Here, we show that a subsecond exposure to a synchrotron X-ray beam is sufficient to fragment the RNA in frozen cells. The method produces hydroxyl radical footprints comparable with those obtained from Fe(II)–EDTA Fenton reactions *in vitro*. The shorter exposure time compared with a ^{137}Cs gamma ray source will permit structural changes to be captured in real time during cell growth.

METHODS

Preparation of cells

E.coli cells (MRE 600) were streaked from a glycerol storage culture on to either M9CA or Luria–Bertani (LB) agar and incubated at 37°C overnight. A single colony was picked to inoculate a starter culture, which was grown at 37°C overnight. The starter culture was used to seed 50–100 ml medium (1/100–1/250 dilution), which was grown with shaking to $OD_{600} = 0.4–0.6$. Cells were chilled by swirling the culture

*To whom correspondence should be addressed. Tel: +1 410 516 2015; Fax: +1 410 516 4118; Email: swoodson@jhu.edu
Present address:
Richard A. Lease, Department of Chemistry and Biochemistry, University of Maryland Baltimore County, 1000 Hilltop Circle, Baltimore, MD 21250, USA

flask in an ice/ethanol bath for 30 s making sure not to freeze the culture. Cells were harvested in pre-chilled 50 ml vials at 5000 r.p.m. (JS13.1 rotor) for 10 min at 4°C, washed with TM buffer (10 mM Tris–HCl, pH 7.5 and 1 mM $MgCl_2$), resuspended in 300 µl TM (~6 µl/µg wet cells or 1.5×10^{11} cells/ml) and snap-frozen as 5–10 µl aliquots in 0.2 ml microcentrifuge tubes in a dry ice/acetone bath. Cells were stored at −80°C until further use.

Exposure to the X-ray beam

Frozen cell pellets were irradiated using facilities at beamline X28C at the National Synchrotron Light Source at Brookhaven National Laboratory. Samples were placed in an aluminum block holder for 0.2 ml tubes, which was maintained at −34 to −38°C with a Cryocool bath. The sample and a Uniblitz XRS6 shutter (Vincent Associates, Rochester, NY) were aligned with the peak of the X-ray beam intensity using a precision motorized table as described previously (20). Individual tubes containing frozen cells were exposed to the X-ray beam for various times ranging from 0 to 2 s. The ring current was 270–300 mA (2.8 GeV). The shutter actuator was used to control the exposure time. When not in the sample holder, the cell pellets were kept frozen in an aluminum block in dry ice for the duration of the experiment. Irradiated cell pellets were compared with three types of controls: cells that were placed in the sample holder but not exposed to the beam (mock treated), cells that were kept frozen outside the experimental hutch, or cells that were kept frozen and not shipped to the beamline.

The 70S ribosomes were isolated from *E.coli* according to published procedures (21) and frozen in 10 µl of 50 mM Tris–HCl, pH 7.5, 150 mM NH_4Cl, 5 mM $MgCl_2$ and 6 mM β-mercaptoethanol at 1 µM final concentration. Frozen samples were exposed to the X-ray beam as described above and stored at −80°C until further analysis. Alternatively, 70S ribosomes were treated in solution with hydroxyl radicals generated by Fe–EDTA complexes as described previously (22).

RNA isolation

Total RNA was isolated from frozen cells by triturating the pellet with 100 µl TRIZOL (Ambion Inc., TX) and extracting with 20 µl chloroform. The aqueous phase was separated by centrifugation at 12 000 *g* for 15 min at 4°C and was extracted once more with TRIZOL and $CHCl_3$. The second extraction was important for obtaining good quality RNA. RNA was precipitated from the final aqueous phase with 100 µl isopropanol for 10 min at room temperature. The RNA collected by centrifugation for 15 min at 12 000 *g* (4°C), washed with 70% ethanol and resuspended in 20 µl RNase-free water. RNA from 70S ribosomes was isolated by phenol:chloroform extraction as described previously (21). The RNA (2 µl) was analyzed on a 1.5% agarose gel prepared in 50 mM Tris–acetate and 1 mM EDTA. RNA concentration was determined by measuring absorbance at 260 nm.

Primer extension

RNA (0.25–0.5 µg) was used for primer extension analysis with ^{32}P-end labeled primers which annealed after nt 161, 560, 1257 and 1508 in the 16S rRNA, 2883 in the 23S rRNA as described previously (23,24), and nt 96–112 in the 5S rRNA. Full-length 16S cDNA was synthesized using a primer that anneals after nt 1508. RNase P RNA was reverse transcribed with 1 µg total RNA and a primer annealing to nt 338–358 as described in Lindell *et al*. (25). The resulting cDNA products were separated on a denaturing 8% polyacrylamide sequencing gel and exposed to a Phosphorimager (Amersham). Dideoxy sequencing reactions were carried out using non-irradiated native rRNA as a template. The observed protection pattern of the 16S rRNA was compared with the solvent-accessible surface area of C4′ atoms computed from coordinates from the structure of the *E.coli* 70S ribosome (*2avy* and *2aw7*) (26), using the program Calc-surf (27).

RESULTS

In vivo radiolysis and RNA cleavage

In vivo footprinting was conducted by exposing *E.coli* to an X-ray beam for various times (Figure 1). *E.coli* MRE 600 were grown to mid-logarithmic phase in either a rich (LB) or minimal (M9CA) medium and rapidly frozen in 5 or 10 µl aliquots containing ~1 µg cells each. The frozen cells remained viable until the time of irradiation, as assessed by the number of colony forming units (data not shown). The tubes containing frozen cells were mounted in a chilled sample holder (−34 to −38°C) and exposed to a 'white light' synchrotron X-ray beam for 0–2 s (Methods). Total RNA was isolated from the irradiated cells and untreated controls. After short exposures, RNA fragments were faintly visible below the 16S rRNA in a 1.5% agarose gel (Figure 2A). After a 1 s exposure, most of the 16S and 23S rRNA was degraded.

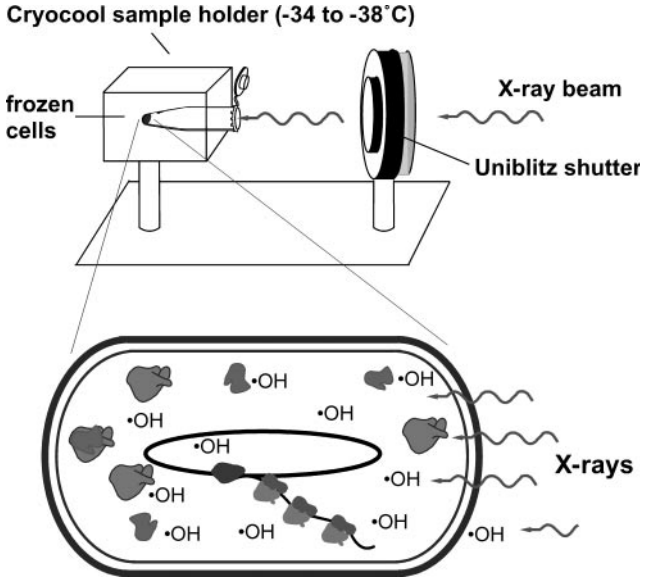

Figure 1. *In vivo* hydroxyl radical footprinting. *E.coli* grown to mid-log phase were concentrated and frozen in 5–10 µl aliquots. Frozen cell pellets were exposed to a 'white light' synchrotron X-ray beam for 0–2 s using a cryostatic sample holder and a programmable shutter at X28C (Brookhaven National Laboratory). Absorption of X-rays by water in the sample generates •OH, which cleaves accessible regions of the RNA backbone. After irradiation, cells were lysed and individual RNAs were analyzed by gene-specific priming of cDNA synthesis.

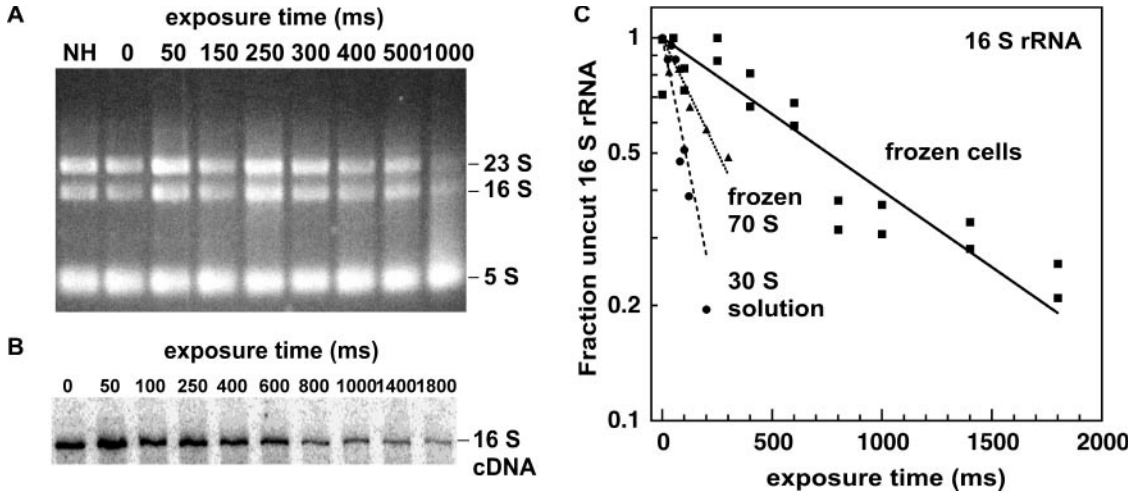

Figure 2. Fragmentation of cellular RNA by X-rays. Total RNA was isolated from frozen *E.coli* (MRE 600) cells after exposure to the X-ray beam for 0–2000 ms. (**A**) Agarose (1.5%) gel electrophoresis of total cellular RNA, strained with ethidium bromide. Exposure times are marked above each lane. Lane NH (no hutch), samples were shipped to the beamline but never placed in the experimental hutch. (**B**) Full-length cDNA of 16S rRNA from irradiated cells. cDNA was synthesized with a ^{32}P-labeled primer and analyzed by denaturing (8%) PAGE. The intensity of the gel bands were quantified using a Phosphorimager. Gel images were scaled and cropped to show the lanes of interest but not otherwise manipulated. (**C**) X-ray dose response curves for hydroxyl radical footprinting. The relative intensity of full-length 16S cDNA from (B) was plotted versus the exposure time and the data were fit to $y = \exp(-kt)$. Symbols: squares, frozen cells (−35°C); triangles, purified 70S ribosomes at −35°C; circles, 30S ribosomal subunits at 37°C.

To determine the optimal X-ray dose for *in vivo* hydroxyl radical footprinting, we measured the exposure time required to cleave 10–30% of the RNA. Under these conditions, individual RNA molecules are cleaved no more than once on average. The extent of cleavage was measured by primer extension, using a molar excess of ^{32}P 5′ end labeled primer complementary to the 3′ end of the 16S rRNA (Figure 2B). The intensity of the cDNA corresponding to the full-length 16S rRNA was plotted versus the exposure time, and the data were fit to an exponential equation (Figure 2C).

A 200–300 ms exposure of cells to the X-ray beam was sufficient to cleave 30% of the 16S rRNA within the frozen cells (Figure 2C). In contrast, a 75–100 ms exposure was sufficient to cleave 25% of the 16S rRNA in purified frozen 70S ribosomes, two to three times longer than the optimal exposure for 30S ribosomes at 37°C (30 ms). Longer exposures may be required to footprint the RNA within frozen cells because of molecular crowding and dehydration of the cytoplasm (less free water) (28), and the presence of free radical scavengers such as cysteine (29). The slower diffusion of free radicals in frozen or supercooled water is also expected to reduce the frequency of strand breaks (30,31).

X-ray footprinting of ribosomes *in vivo*

In vivo hydroxyl radical cleavage patterns of the 16S, 23S and 5S rRNA and RNase P M1 RNA were mapped by extension of primers complementary to specific RNA templates with reverse transcriptase. As illustrated for the 16S rRNA in Figure 3, the exposure times required for obtaining footprints in the 5′ domain correlated well with the X-ray dose needed to cleave ∼20% of the RNA. After 200 ms exposure, protected sequences were clearly visible and could be assigned by comparison with a dideoxy-sequencing ladder. We were also able to visualize footprints on specific regions of the 23S and 5S rRNA using primers that anneal to those RNAs (data not shown). The footprinting pattern after irradiation was comparable with that obtained by treatment of ribosomes with Fe(II)–EDTA (data not shown) (22). This supports the idea that cleavage *in vivo* is primarily caused by attack of hydroxyl radical on the RNA backbone. Although the nucleobases also react with •OH, such base damage infrequently results in cleavage of the phosphodiester backbone (13,32,33). Moreover, common base lesions such as 8-oxo-G are not expected to prevent the passage of reverse transcriptase (34).

Conformation of ribosomes *in vitro* and *in vivo*

The pattern of RNA backbone protection in frozen cells was similar to that observed in the isolated 70S ribosomes for most of the regions analyzed in our initial experiments (Figure 3). Moreover, the regions of the 16S rRNA protected from cleavage correlated with the surface accessibility of ribose atoms (data not shown) calculated from crystal structures of the *E.coli* 70S ribosome (26). Additional nucleotides were protected from cleavage *in vivo*, however, as illustrated in Figure 4. For example, residue 1229 in the 3′ domain of the 16S rRNA is more protected *in vivo* than in empty 70S ribosomes (Figure 4A). This protection can be explained by the direct interaction of 16S rRNA with the anticodon stem of the peptidyl tRNA, which is augmented by interactions with the extended C-terminal of ribosomal protein S13 (35).

Not all of the local differences between the *in vivo* and *in vitro* footprints can be explained by direct interactions of ligands with the rRNA. For example, residues 1225–1227 were also protected much more strongly *in vivo* although these protections result from the interaction of the 16S rRNA with S13 (36), which is present in purified 70S ribosomes. Similarly, nt 492, 493 and 498, 499, 501 and 507 are more protected *in vivo* relative to 70S ribosomes *in vitro*, while nt 497 is cleaved more strongly *in vivo* (Figure 4B). These residues surround a 5-helix junction in the 5′ domain of 16S rRNA,

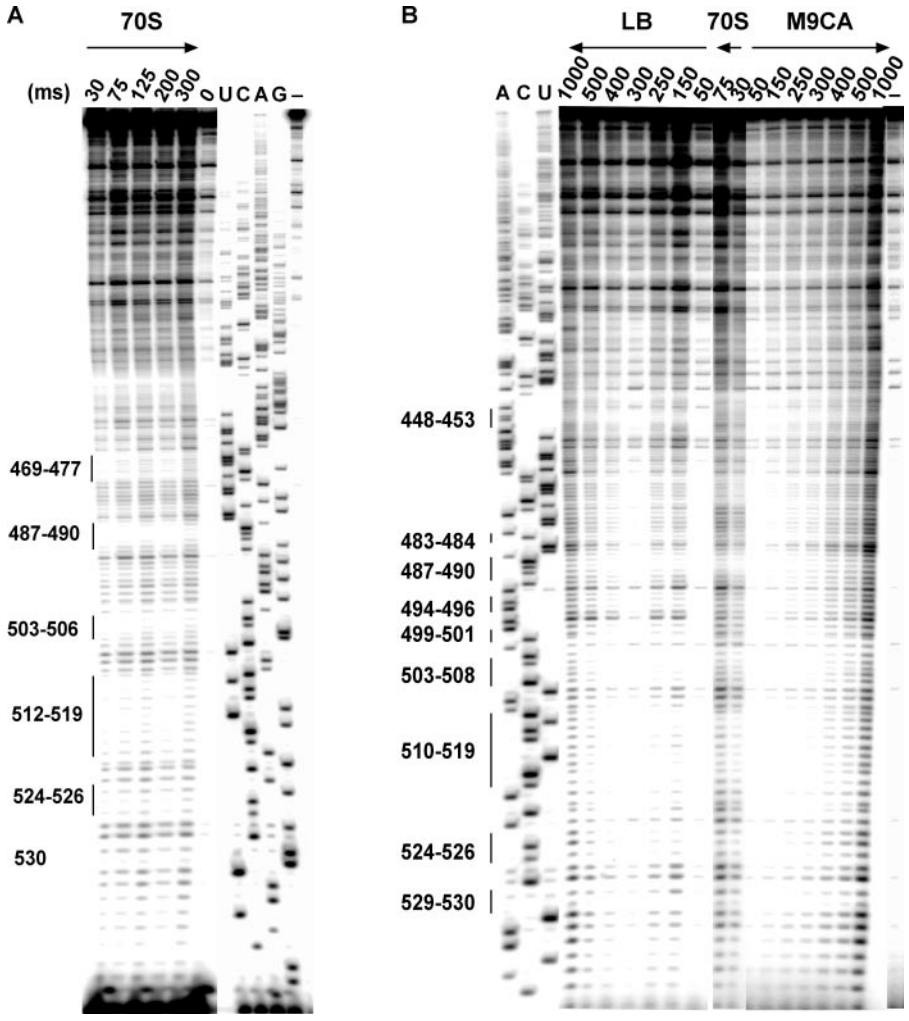

Figure 3. *In vivo* footprinting of 16S rRNA by primer extension. cDNA synthesis on RNA from irradiated cells was primed with a ^{32}P-labeled oligonucleotide annealing after nt 560 in *E.coli* 16S rRNA. Products were compared with standard dideoxy sequencing ladders on 8% sequencing gels. (**A**) Hydroxyl radical protection pattern of 16S rRNA from purified, frozen 70S ribosomes. Exposure times in milliseconds are indicated above the lanes; lanes U, C, A and G represent dideoxy sequencing reactions; minus, control reaction on unexposed rRNA that was not shipped to the beamline. Some of the protected regions are indicated on the left. (**B**) Intracellular footprinting of 16S rRNA. *E.coli* were grown in LB or M9CA media and exposed to the X-ray beam for the times shown (Methods). 70S, *in vitro* exposures as in (A).

which is the binding site of ribosomal protein S4. Such differences in the extent of cleavage may arise from perturbation of the ribosome's structure during translation. It is also conceivable that small molecules within the cytoplasm sensitize certain bases to radiation damage, although this would not explain why most nucleotides have the same relative sensitivity to X-ray induced cleavage in the bacterium and in purified ribosomes.

To determine the extent to which immature ribosomal subunits may contribute to our *in vivo* footprinting results, a primer that anneals close to the 5′ end of the 16S rRNA was extended across the 5′ leader (data not shown). The unprocessed 35S and the pre-16S rRNAs were 1 and 8.5% as abundant as the mature 16S rRNA, based on the intensities of cDNA bands terminating at the 5′ end of the leader and the RNase III cleavage site (pre-16S rRNA), respectively. These results are similar to previously published values (37). Since the pre-rRNA is one-tenth as abundant as the mature rRNA, the latter presumably dominates the footprints on the mature sequences.

In vivo footprinting of RNase P

Using this technique, we were also able to probe the structure of the M1 RNA subunit of RNase P, which is ~100-fold less abundant than rRNA (~1000 copies/cell) during rapid growth (38). Because of the lower amount of M1 RNA in our samples, the signal to noise ratio was less favorable than for the rRNA. Nonetheless, reverse transcription with a primer that anneals to the 3′ end of M1 RNA revealed the protection of residues in P6, P17, P16 and L15 (Figure 5A). These nucleotides are involved in tertiary interactions within M1 RNA or with the pre-tRNA (39), and have been shown to be protected from Fe–EDTA-dependent hydroxyl radical cleavage in the presence of ligands (40). The optimal exposure time for M1 RNA was 200–300 ms, as it was for the 16S rRNA (Figure 5B).

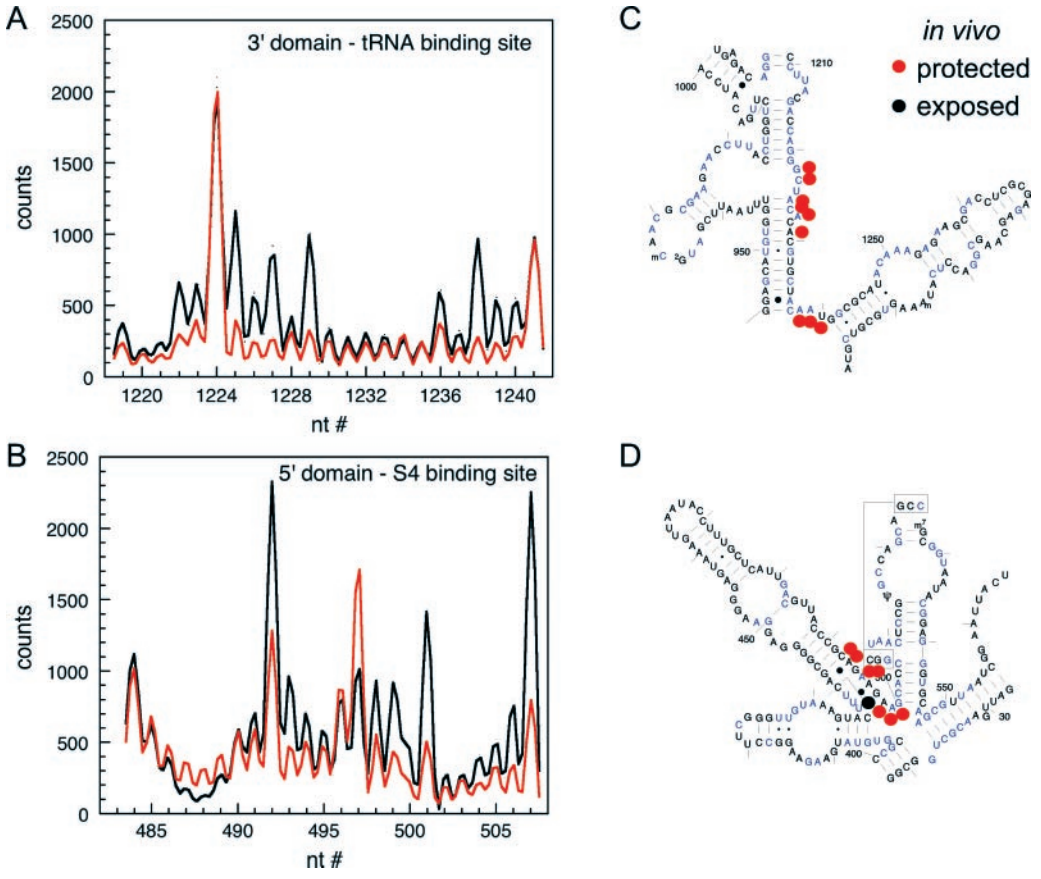

Figure 4. Comparison of *in vivo* and *in vitro* footprinting of 16S rRNA. The intensity of bands in sequencing gels (Figure 3) were quantified using a phosphorimager. (**A**) nt 1218–1242 in the 16S 3′ domain. (**B**) nt 483–508 in the 5′ domain. Red lines, irradiation *in vivo* (250 ms exposure); black lines, irradiation *in vitro* (30 ms exposure). Lane profiles were scaled by matching the intensity of peaks from intrinsic RT pauses. (**C** and **D**) Differences in cleavage protection. Red circles, greater protection *in vivo* than *in vitro*; black circle, enhanced cleavage *in vivo*. Blue letters indicate residues with predicted low backbone accessibility, based on crystallographic coordinates.

DISCUSSION

Despite the many advances in structural biology, few available methods can capture the structural dynamics of cellular complexes within the cell. *In vivo* footprinting is important because it corroborates molecular structures determined *in vitro*, and can provide structural information on complexes that are not easily purified or reconstituted biochemically. Because cleavage by hydroxyl radical depends on the solvent accessibility of the DNA or RNA backbone, it is particularly useful for deducing 3D structure or mapping nucleic acid–protein interactions.

We show that hydroxyl radical footprinting can be carried out on RNA–protein complexes in living cells using a synchrotron X-ray beam. In general, the results correlate well with those of 'X-ray' and Fe(II)–EDTA footprinting experiments *in vitro*. A similar correspondence between *in vitro* and *in vivo* cleavage patterns was reported in previous experiments using a ^{137}Cs gamma ray source to footprint protein–DNA complexes *in vivo* (19). The advantages of using a synchrotron X-ray beam to footprint nucleic acids *in vivo* are the excellent penetration of intact cells and tissue samples, the relatively short exposure times (0.2 s) and the ability to precisely control the extent of cleavage by adjusting the exposure time.

We find the method to be robust and relatively insensitive to small variations in exposure time, cell handling or sample size. The signal-to-noise ratio of the footprinting results, however, was sensitive to the quality of the RNA after isolation. We obtained the best results by washing cell pellets in Tris–magnesium buffer before freezing to stabilize the membranes and to remove residual media. It was essential to keep cells completely frozen until extraction of the RNA to prevent its degradation by nucleases. We obtained better primer extension data by isolating RNA with Trizol than with silica resins.

Flash freezing cells before irradiation makes it possible to take 'snapshots' of macromolecules in various stages of metabolism, while stabilizing cells against heat damage. The bacterial cytoplasm is expected to remain frozen during exposure to the X-ray beam at −35°C (28), although there may have been local thawing due to the absorption of X-rays. The slightly longer exposure times needed to footprint ribosomes in frozen buffer compared with solution suggest that freezing inhibits but does not prevent cleavage of macromolecules by hydroxyl radical. Although photophysical events like the formation of hydroxyl radicals and aqueous electrons occur at low temperatures, hydroxyl radicals diffuse more slowly in vitreous ice or supercooled water, reducing

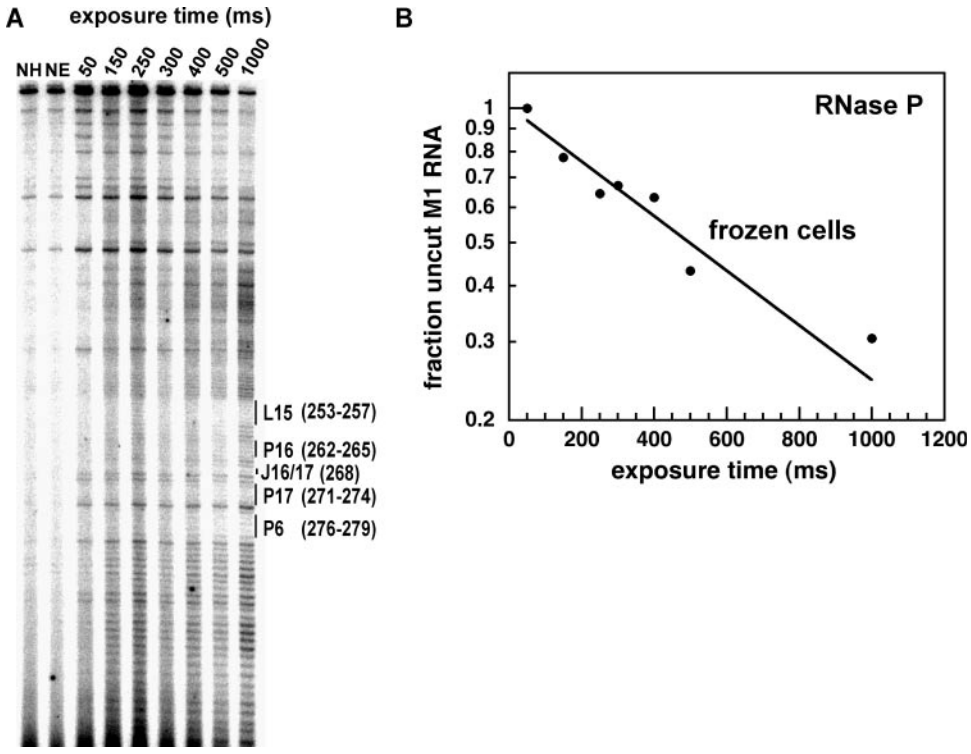

Figure 5. *In vivo* footprinting of *E.coli* RNase P. (**A**) Primer extension reactions were analyzed on sequencing gels as in Figure 3. Protected regions of the M1 RNA (right) were assigned by counting bands from the 3′ end of the primer, and compared well with published results. Lanes NH (no hutch), cells never entered the experimental hutch; NE (no exposure), cells were placed in the sample block but not exposed to the beam (mock treated). (**B**) Dose–response curve, as in Figure 2.

the extent of strand cleavage (28). Nonetheless, in hydrated DNA at −196°C most of the radiation damage is attributed to indirect events (hydroxyl radical) rather than the direct absorption of X-rays (30,31,41). We obtained comparable footprints by irradiation of frozen and thawed samples and from Fe-EDTA treatment of 70S ribosomes in solution. This suggests that the accessibility of the RNA backbone to hydroxyl radical primarily determined the cleavage pattern in frozen cell pellets, as expected.

Many RNPs undergo significant structural changes during their lifecycle. For example, ribosomal subunits undergo irreversible conformational changes during their maturation, and reversible conformational changes during initiation, elongation and termination of protein synthesis. The *in vivo* footprints presented here represent the average conformational state of the 16S rRNA within the cell at a certain growth rate. In the future, it may be possible to analyze specific RNP subpopulations using sequence tags, selective markers or temperature-sensitive mutations.

Because X-rays easily penetrate intact cells and even whole tissues, we expect this method to be applicable to a wide range of biological systems. The relatively short irradiation times and the ability to use frozen cells would enable this method to visualize changes in cell components after viral infection or during the course of development. The range of potential footprinting applications could be increased by the use of electrospray mass spectrometry to footprint proteins (42) or ligation-mediated PCR to amplify footprinting patterns of single-copy genes or low-abundance mRNAs in eukaryotic cells (43). Thus, *in vivo* X-ray-dependent hydroxyl radical footprinting offers a new approach for obtaining detailed information about the three-dimensional structure of nucleic acids *in situ*.

ACKNOWLEDGEMENTS

The authors wish to thank M. Brenowitz, S. Gupta and M. Sullivan for assistance with beamline experiments and construction of the cooled sample holder; M. Deras and S. Koduvayur for help with initial experiments and P. Fleming for assistance with accessible surface area calculations. This work was supported by a grant from the NIH (GM60809). Beamline X28C is operated by the Center for Synchrotron Biosciences and supported by the NIH. The Open Access publication charges for this article were waived by Oxford University Press—*NAR* Editorial Board members are entitled to one free paper per year in recognition of their work on behalf of the journal.

Conflict of interest statement. None declared.

REFERENCES

1. Climie,S.C. and Friesen,J.D. (1988) *In vivo* and *in vitro* structural analysis of the rplJ mRNA leader of *Escherichia coli*. Protection by bound L10-L7/L12. *J. Biol. Chem.*, **263**, 15166–15175.
2. Lindell,M., Romby,P. and Wagner,E.G. (2002) Lead(II) as a probe for investigating RNA structure *in vivo*. *RNA*, **8**, 534–541.

3. Mayford,M. and Weisblum,B. (1989) Conformational alterations in the ermC transcript *in vivo* during induction. *EMBO J.*, **8**, 4307–4314.
4. Zaug,A.J. and Cech,T.R. (1995) Analysis of the structure of Tetrahymena nuclear RNAs *in vivo*: telomerase RNA, the self-splicing rRNA intron, and U2 snRNA. *RNA*, **1**, 363–374.
5. Wells,S.E., Hughes,J.M., Igel,A.H. and Ares,M.,Jr (2000) Use of dimethyl sulfate to probe RNA structure *in vivo*. *Methods Enzymol.*, **318**, 479–493.
6. Balzer,M. and Wagner,R. (1998) A chemical modification method for the structural analysis of RNA and RNA–protein complexes within living cells. *Anal. Biochem.*, **256**, 240–242.
7. Waldsich,C., Grossberger,R. and Schroeder,R. (2002) RNA chaperone StpA loosens interactions of the tertiary structure in the td group I intron *in vivo*. *Genes Dev.*, **16**, 2300–2312.
8. Sasse-Dwight,S. and Gralla,J.D. (1989) KMnO4 as a probe for lac promoter DNA melting and mechanism *in vivo*. *J. Biol. Chem.*, **264**, 8074–8081.
9. Basak,S. and Nagaraja,V. (2001) A versatile *in vivo* footprinting technique using 1,10-phenanthroline–copper complex to study important cellular processes. *Nucleic Acids Res.*, **29**, E105–E105.
10. Tullius,T.D. and Greenbaum,J.A. (2005) Mapping nucleic acid structure by hydroxyl radical cleavage. *Curr. Opin. Chem. Biol.*, **9**, 127–134.
11. Sclavi,B., Sullivan,M., Chance,M.R., Brenowitz,M. and Woodson,S.A. (1998) RNA folding at millisecond intervals by synchrotron hydroxyl radical footprinting. *Science*, **279**, 1940–1943.
12. Klassen,N.V. (1987) Primary products in radiation chemistry. In Farhatazis,I. and Rodgers,M.A. (eds), *Radiation Chemistry: Principles and Applications*. VCH Publications, TX, pp. 29–61.
13. Dizdaroglu,M. and Bergtold,D.S. (1986) Characterization of free radical-induced base damage in DNA at biologically relevant levels. *Anal. Biochem.*, **156**, 182–188.
14. von Sonntag,C. (1991) The chemistry of free-radical-mediated DNA damage. *Basic Life Sci.*, **58**, 287–317; Discussion 317–221.
15. Balasubramanian,B., Pogozelski,W.K. and Tullius,T.D. (1998) DNA strand breaking by the hydroxyl radical is governed by the accessible surface areas of the hydrogen atoms of the DNA backbone. *Proc. Natl Acad. Sci. USA*, **95**, 9738–9743.
16. Latham,J.A. and Cech,T.R. (1989) Defining the inside and outside of a catalytic RNA molecule. *Science*, **245**, 276–282.
17. Cate,J.H., Gooding,A.R., Podell,E., Zhou,K., Golden,B.L., Kundrot,C.E., Cech,T.R. and Doudna,J.A. (1996) Crystal structure of a group I ribozyme domain: principles of RNA packing. *Science*, **273**, 1678–1685.
18. Adams,P.L., Stahley,M.R., Gill,M.L., Kosek,A.B., Wang,J. and Strobel,S.A. (2004) Crystal structure of a group I intron splicing intermediate. *RNA*, **10**, 1867–1887.
19. Ottinger,L.M. and Tullius,T.D. (2000) High resolution *in vivo* footprinting of a protein–DNA complex using gamma radiation. *J. Am. Chem. Soc.*, **122**, 5901–5902.
20. Dhavan,G.M., Chance,M.R. and Brenowitz,M. (2003) Kinetics analysis of DNA–protein interactions by time resolved synchrotron X-ray footprinting. In Johnson,K.A. (ed.), *Kinetic Analysis of Macromolecules: A Practical Approach*. IRL Press at Oxford University, Oxford, pp. 75–86.
21. Nierhaus,K.H. and Dohme,F. (1974) Total reconstitution of functionally active 50S ribosomal subunits from *Escherichia coli*. *Proc. Natl Acad. Sci. USA*, **71**, 4713–4717.
22. Merryman,C., Moazed,D., McWhirter,J. and Noller,H.F. (1999) Nucleotides in 16S rRNA protected by the association of 30S and 50S ribosomal subunits. *J. Mol. Biol.*, **285**, 97–105.
23. Moazed,D., Stern,S. and Noller,H.F. (1986) Rapid chemical probing of conformation in 16 S ribosomal RNA and 30 S ribosomal subunits using primer extension. *J. Mol. Biol.*, **187**, 399–416.
24. Merryman,C. and Noller,H.F. (1998) Footprinting and modification-interference analysis of binding sites on RNA. In Smith,C.W.J. (ed.), *RNA–Protein Interactions*. Oxford University Press, NY, pp. 237–253.
25. Lindell,M., Brannvall,M., Wagner,E.G. and Kirsebom,L.A. (2005) Lead(II) cleavage analysis of RNase P RNA *in vivo*. *RNA*, **11**, 1348–1354.
26. Schuwirth,B.S., Borovinskaya,M.A., Hau,C.W., Zhang,W., Vila-Sanjurjo,A., Holton,J.M. and Cate,J.H. (2005) Structures of the bacterial ribosome at 3.5 A resolution. *Science*, **310**, 827–834.
27. Gerstein,M. (1992) A resolution-sensitive procedure for comparing protein surfaces and its application to the comparison of antigen-combining sites. *Acta Cryst. A*, **48**, 271–276.
28. Mazur,P. (1984) Freezing of living cells: mechanisms and implications. *Am. J. Physiol.*, **247**, C125–142.
29. Roberts,J.C., Koch,K.E., Detrick,S.R., Warters,R.L. and Lubec,G. (1995) Thiazolidine prodrugs of cysteamine and cysteine as radioprotective agents. *Radiat. Res.*, **143**, 203–213.
30. Huttermann,J., Rohrig,M. and Kohnlein,W. (1992) Free radicals from irradiated lyophilized DNA: influence of water of hydration. *Int. J. Radiat. Biol.*, **61**, 299–313.
31. Ohshima,H., Iida,Y., Matsuda,A. and Kuwabara,M. (1996) Damage induced by hydroxyl radicals generated in the hydration layer of gamma-irradiated frozen aqueous solution of DNA. *J. Radiat. Res. (Tokyo)*, **37**, 199–207.
32. Duplaa,A.M. and Teoule,R. (1985) Sites of gamma radiation-induced DNA strand breaks after alkali treatment. *Int. J. Radiat. Biol. Relat. Stud. Phys. Chem. Med.*, **48**, 19–32.
33. Cadet,J., Bellon,S., Douki,T., Frelon,S., Gasparutto,D., Muller,E., Pouget,J.P., Ravanat,J.L., Romieu,A. and Sauvaigo,S. (2004) Radiation-induced DNA damage: formation, measurement, and biochemical features. *J. Environ. Pathol. Toxicol. Oncol.*, **23**, 33–43.
34. Hogg,M., Wallace,S.S. and Doublie,S. (2005) Bumps in the road: how replicative DNA polymerases see DNA damage. *Curr. Opin. Struct. Biol.*, **15**, 86–93.
35. Yusupov,M.M., Yusupova,G.Z., Baucom,A., Lieberman,K., Earnest,T.N., Cate,J.H. and Noller,H.F. (2001) Crystal structure of the ribosome at 5.5 A resolution. *Science*, **292**, 883–896.
36. Brodersen,D.E., Clemons,W.M.,Jr, Carter,A.P., Wimberly,B.T. and Ramakrishnan,V. (2002) Crystal structure of the 30 S ribosomal subunit from Thermus thermophilus: structure of the proteins and their interactions with 16 S RNA. *J. Mol. Biol.*, **316**, 725–768.
37. King,T.C. and Schlessinger,D. (1983) S1 nuclease mapping analysis of ribosomal RNA processing in wild type and processing deficient *Escherichia coli*. *J. Biol. Chem.*, **258**, 12034–12042.
38. Dong,H., Kirsebom,L.A. and Nilsson,L. (1996) Growth rate regulation of 4.5 S RNA and M1 RNA the catalytic subunit of *Escherichia coli* RNase P. *J. Mol. Biol.*, **261**, 303–308.
39. Torres-Larios,A., Swinger,K.K., Krasilnikov,A.S., Pan,T. and Mondragon,A. (2005) Crystal structure of the RNA component of bacterial ribonuclease P. *Nature*, **437**, 584–587.
40. Westhof,E., Wesolowski,D. and Altman,S. (1996) Mapping in three dimensions of regions in a catalytic RNA protected from attack by an Fe(II)–EDTA reagent. *J. Mol. Biol.*, **258**, 600–613.
41. Gregoli,S., Olast,M. and Bertinchamps,A. (1982) Radiolytic pathways in gamma-irradiated DNA: influence of chemical and conformational factors. *Radiat. Res.*, **89**, 238–254.
42. Maleknia,S.D., Brenowitz,M. and Chance,M.R. (1999) Millisecond radiolytic modification of peptides by synchrotron X-rays identified by mass spectrometry. *Anal. Chem.*, **71**, 3965–3973.
43. Grange,T., Bertrand,E., Espinas,M.L., Fromont-Racine,M., Rigaud,G., Roux,J. and Pictet,R. (1997) *In vivo* footprinting of the interaction of proteins with DNA and RNA. *Methods*, **11**, 151–163.